ATLAS NOTE

ATLAS-CONF-2012-072

June 29, 2012

Search for Diphoton Events with Large Missing Transverse Momentum in 7 TeV pp Collision Data with the ATLAS Detector

The ATLAS Collaboration

Abstract

A search for diphoton events with large missing transverse momentum has been performed using 4.8 fb^{-1} of proton–proton collision data at $\sqrt{s}$ = 7 TeV recorded with the ATLAS detector. No excess of events was observed above the Standard Model prediction and model-dependent 95 % confidence level exclusion limits are set. In the context of a generalised model of gauge-mediated supersymmetry breaking with a bino-like lightest neutralino of mass above 50 GeV, gluinos (squarks) below 1.07 TeV (0.91 TeV) are excluded, while a breaking scale Λ below 203 TeV is excluded for a minimal model of gauge-mediated supersymmetry breaking. For a specific model with one universal extra dimension, compactification scales $1/R < 1.41$ TeV are excluded.

ATLAS-CONF-2012-072
06 July 2012

1 Introduction

This note reports on the search for diphoton ($\gamma\gamma$) events with large missing transverse momentum ($E_{\mathrm{T}}^{\mathrm{miss}}$) in 4.8 fb^{-1} of proton–proton (pp) collision data at $\sqrt{s} = 7$ TeV recorded with the ATLAS detector at the Large Hadron Collider (LHC) in 2011, extending and superseding a prior study performed with 1 fb^{-1} [1]. The results are interpreted in the context of three models of new physics: a general model of gauge-mediated supersymmetry breaking (GGM) [2–4], a minimal model of gauge-mediated supersymmetry breaking (SPS8) [5], and a model with one universal extra dimension (UED) [6–8].

2 Supersymmetry

Supersymmetry (SUSY) [9–17] introduces a symmetry between fermions and bosons, resulting in a SUSY partner (sparticle) with identical quantum numbers except a difference of half a unit of spin for each Standard Model (SM) particle. As none of these sparticles have been observed, SUSY must be a broken symmetry if realised in nature. Assuming R-parity conservation [18–22], sparticles have to be produced in pairs. These would then decay through cascades involving other sparticles until the lightest SUSY particle (LSP) is produced, which is stable.

In gauge-mediated SUSY breaking (GMSB) models [23–28] the LSP is the gravitino $\tilde{G}$. GMSB experimental signatures are largely determined by the nature of the next-to-lightest SUSY particle (NLSP). In this study the NLSP is assumed to be the lightest neutralino $\tilde{\chi}_1^0$. For studies with the lightest stau as NLSP see Refs. [29, 30]. Should the lightest neutralino be a "bino", with couplings identical to those of the SM U(1) gauge boson, the final decay in the cascade would predominantly be $\tilde{\chi}_1^0 \rightarrow \gamma\tilde{G}$, with two cascades per event, leading to final states with $\gamma\gamma + E_{\mathrm{T}}^{\mathrm{miss}}$, where $E_{\mathrm{T}}^{\mathrm{miss}}$ results from the undetected gravitinos.

Two different classes of gauge-mediated models, described in more detail below, are considered: the minimal GMSB model (SPS8) as an example of a complete SUSY model with a full particle spectrum and two different variants of the GGM model as an example of a phenomenological model with reduced particle content.

In the SPS8 model, the only free parameter is the SUSY breaking mass scale Λ felt by the low-energy sector. The other model parameters are fixed to the following values: the messenger mass $M_{\mathrm{mess}} = 2\Lambda$, the number of SU(5) messengers $N_5 = 1$, the ratio of the vacuum expectation values of the two Higgs doublets $\tan\beta = 15$, and the Higgs sector mixing parameter $\mu > 0$. The bino NLSP is assumed to decay promptly ($c\tau_{\mathrm{NLSP}} < 0.1$ mm). For $\Lambda \simeq 200$ TeV, the direct production of gaugino pairs such as $\tilde{\chi}_2^0\,\tilde{\chi}_1^{\pm}$ or $\tilde{\chi}_1^+\,\tilde{\chi}_1^-$ pairs is expected to dominate at an LHC centre-of-mass energy of $\sqrt{s} = 7$ TeV. The contribution from gluino and/or squark pairs is below 10 % of the production cross section due to their high masses. The sparticle pair produced in the collision decays via cascades into two photons and two gravitinos. Further SM particles such as gluons, quarks, leptons and gauge bosons may be produced in the cascade decays. The current best limit on Λ in this model is 145 TeV [1].

Two different configurations of the GGM SUSY model are considered in this study, for which the neutralino NLSP, chosen to be the bino, and either the gluino or the squark masses are treated as free parameters. For the gluino-bino model all squark masses are decoupled (set to inaccessibly large values). For the squark-bino GGM model all squark masses are treated as degenerate except the right-handed up-type squarks whose mass is decoupled. For both configurations all other sparticle masses are also decoupled, leading to a dominant production mode at $\sqrt{s} = 7$ TeV of a pair of gluinos in one case and a pair of squarks in the other case. These would decay via short cascades into the bino-like neutralino NLSP. Jets may be produced in the cascades from the gluino and squark decays. Further model parameters are fixed to $\tan\beta = 2$ and $c\tau_{\mathrm{NLSP}} < 0.1$ mm. The decay into the wino-like neutralino NLSP is also possible and was studied by the CMS Collaboration [31].

3 Extra dimensions

UED models postulate the existence of additional spatial dimensions in which all SM particles can propagate, leading to the existence of a series of excitations for each SM particle, known as a Kaluza-Klein (KK) tower. This analysis considers the case of a single UED, with compactification radius (size of the extra dimension) $R \approx 1\,\text{TeV}^{-1}$. At the LHC, the main UED process would be the production via the strong interaction of a pair of first-level KK quarks and/or gluons [32]. These would decay via cascades involving other KK particles until reaching the lightest KK particle (LKP), i.e. the first level KK photon γ^*. SM particles such as quarks, gluons, leptons, and gauge bosons may be produced in the cascades. If the UED model is embedded in a larger space with N additional eV^{-1}-sized dimensions accessible only to gravity [33], with a $(4 + N)$-dimensional Planck scale (M_D) of a few TeV, the LKP would undergo a prompt gravitational decay to $\gamma^* \to \gamma + G$. G represents a tower of eV-spaced graviton states, leading to a graviton mass between 0 and $1/R$. With two decay chains per event, the final state would contain $\gamma\gamma + E_{\text{T}}^{\text{miss}}$, where $E_{\text{T}}^{\text{miss}}$ results from the escaping gravitons. Up to $1/R \sim 1\,\text{TeV}$, the branching ratio to the diphoton and $E_{\text{T}}^{\text{miss}}$ final state is close to 100 %. As $1/R$ increases, the gravitational decay widths become more important for all KK particles and the branching ratio into photons decreases, e.g. to 50 % for $1/R = 1.5\,\text{TeV}$ [7].

The UED model considered here is defined by specifying R and Λ, the ultraviolet cut-off used in the calculation of radiative corrections to the KK masses. This analysis sets Λ such that $\Lambda R = 20$ [34]. The γ^* mass is insensitive to Λ, while other KK masses typically change by a few per cent when varying ΛR in the range $10 - 30$. For $1/R = 1400\,\text{GeV}$, the masses of the first-level KK photon, quark, and gluon are 1400, 1615 and 1708 GeV, respectively [35].

4 Simulated samples

For the GGM model, the SUSY mass spectra were calculated using `SUSPECT` 2.41 [36] and `SDECAY` 1.3 [37]; for the SPS8 model, the SUSY mass spectra were calculated using `ISAJET` 7.80 [38]. The Monte Carlo (MC) SUSY signal samples were produced using `HERWIG++` 2.5.1 [39] with `MRST2007 LO*` [40] parton distribution functions (PDF). Signal cross sections are calculated to next-to-leading order (NLO) in the strong coupling constant, including the resummation of soft gluon emission at next-to-leading-logarithmic accuracy (NLO+NLL) [41–45]. The nominal cross section and the uncertainty are taken from an envelope of cross section predictions using different PDF sets and factorisation and renormalisation scales, as described in Ref. [46]. In the case of the UED model, cross sections were estimated and MC signal samples generated using the UED model as implemented at leading order (LO) in `PYTHIA` 6.423 [35, 47] with `MRST2007 LO*` PDF.

The "irreducible" background from $W(\to \ell\nu) + \gamma\gamma$ and $Z(\to \nu\bar{\nu}) + \gamma\gamma$ production was simulated at LO using `MadGraph` 4 [48] with the `CTEQ6L1` [49] PDF. Parton showering and fragmentation were simulated with `PYTHIA`. NLO cross sections and scale uncertainties were used via K-factor [50, 51]. These are 2.0 ± 0.3 for $Z(\to \nu\bar{\nu}) + \gamma\gamma$ and 3 ± 3 for $W(\to \ell\nu) + \gamma\gamma$ production. As will be described below, all other background sources are estimated through the use of control samples derived from data.

All samples were processed through the `GEANT4`-based simulation [52] of the ATLAS detector [53]. The variation of the number of pp interactions per bunch crossing (pile-up) as a function of the instantaneous luminosity is taken into account by overlaying simulated minimum bias events according to the observed distribution of the number of pile-up interactions in data, with an average of ~ 10 interactions.

5 ATLAS detector

The ATLAS detector [54] is a multi-purpose apparatus with a forward-backward symmetric cylindrical geometry and nearly 4π solid angle coverage[1]. Closest to the beamline are tracking devices comprised of layers of silicon-based pixel and strip detectors covering $|\eta| < 2.5$ and straw-tube detectors covering $|\eta| < 2.0$, located inside a thin superconducting solenoid that provides a 2 T magnetic field. Outside the solenoid, fine-granularity lead/liquid-argon electromagnetic (EM) calorimeters provide coverage for $|\eta| < 3.2$ to measure the energy and position of electrons and photons. A presampler, covering $|\eta| < 1.8$, is used to correct for energy lost upstream of the EM calorimeter. An iron/scintillating-tile hadronic calorimeter covers the region $|\eta| < 1.7$, while copper and liquid-argon technology is used for hadronic calorimeters in the end-cap region $1.5 < |\eta| < 3.2$. In the forward region $3.2 < |\eta| < 4.9$ liquid-argon calorimeters with copper and tungsten absorbers measure the electromagnetic and hadronic energy. A muon spectrometer consisting of three superconducting toroidal magnet systems each comprised of eight toroidal coils, tracking chambers, and detectors for triggering surrounds the calorimeter system.

6 Reconstruction of candidates and observables

The reconstruction of converted and unconverted photons and of electrons is described in Refs. [55] and [56], respectively. Photon candidates were required to be within $|\eta| < 1.81$, and to be outside the transition region $1.37 < |\eta| < 1.52$ between the barrel and the end-cap calorimeters. Identified on the basis of the characteristics of the longitudinal and transverse shower development in the EM calorimeter, the analysis made use of both "loose" and "tight" photons [55]. Photon candidates were removed if they were found to be within $\Delta R < 0.01$ of an electron candidate, where $\Delta R = \sqrt{\Delta\eta^2 + \Delta\phi^2}$ is the separation between the electron and photon candidates in $\eta - \phi$ space. In addition, converted photons were re-classified as electrons if one or more candidate conversion tracks included at least one hit from the pixel layers. Giving preference to the electron selection in this way reduced the electron-to-photon fake rate by $50 - 60\%$ (depending on the value of η) relative to that of the prior 1 fb^{-1} analysis [1], while preserving over 70% of the signal efficiency. Finally, an "isolation" requirement was imposed, whereby photon candidates were removed if more than 5 GeV of transverse energy was observed in a cone of $\Delta R < 0.2$ surrounding the photon's deposition in the calorimeter, after correcting for contributions from pile-up and the deposition ascribed to the photon itself.

The measurement of the two-dimensional transverse momentum vector $\mathbf{p}_{\mathrm{T}}^{\mathrm{miss}}$ (and its magnitude $E_{\mathrm{T}}^{\mathrm{miss}}$) is based on energy deposits in calorimeter cells inside three-dimensional clusters with $|\eta| < 4.9$ and is corrected for contributions from muons, if any [57]. The cluster energy is calibrated to correct for the different response to electromagnetically- and hadronically-induced showers, energy loss in dead material, and out-of-cluster energy.

Jets were reconstructed using the anti-k_t jet algorithm [58] with four-momentum recombination and radius parameter $R = 0.4$. They were required to have $p_{\mathrm{T}} > 20$ GeV and $|\eta| < 2.8$.

Two additional observables of use in discriminating SM backgrounds from potential GMSB and UED signals were defined. The total visible transverse energy H_{T} was calculated as the sum of the magnitude of the transverse momenta of the two selected photons and any additional leptons and jets in the event. The photon-$E_{\mathrm{T}}^{\mathrm{miss}}$ separation $\Delta\phi(\gamma, E_{\mathrm{T}}^{\mathrm{miss}})$ was defined as the azimuthal angle between the missing transverse momentum vector and either of the two selected photons, with $\Delta\phi_{\mathrm{min}}(\gamma, E_{\mathrm{T}}^{\mathrm{miss}})$ the minimum value of $\Delta\phi(\gamma, E_{\mathrm{T}}^{\mathrm{miss}})$ of the two selected photons.

[1] ATLAS uses a right-handed coordinate system with its origin at the nominal interaction point (IP) in the centre of the detector and the z-axis along the beam pipe. The x-axis points from the IP to the centre of the LHC ring, and the y-axis points upward. Cylindrical coordinates (R, ϕ) are used in the transverse plane, ϕ being the azimuthal angle around the beam pipe. The pseudorapidity is defined in terms of the polar angle θ as $\eta = -\ln\tan(\theta/2)$.

7 Data analysis

The data sample, corresponding to an integrated luminosity of $4.8 \pm 0.2\,\text{fb}^{-1}$ [59, 60], was selected by a trigger requiring two loose photon candidates with $E_{\text{T}} > 20\,\text{GeV}$. To ensure that activity recorded in the event resulted from a beam collision, events were required to have at least one vertex with more than four associated tracks. Events were then required to contain at least two tight photon candidates with $E_{\text{T}} > 50\,\text{GeV}$, which MC studies suggested would provide the greatest separation between signal and SM background for a broad range of the parameter space of the new physics scenarios under consideration in this search. A total of 10455 isolated $\gamma\gamma$ candidate events passing these selection requirements were observed in the data sample. The E_{T} distributions[2] of the leading and sub-leading photon for events in this sample are shown in Figs. 1 and 2. Also shown are the E_{T} spectra obtained from GGM MC samples for $m_{\tilde{g}} = 1000\,\text{GeV}$ and $m_{\tilde{\chi}_1^0} = 450\,\text{GeV}$, from SPS MC samples for $\Lambda = 190\,\text{TeV}$, and from UED MC samples for $1/R = 1.3\,\text{TeV}$, representing model parameters near the expected exclusion limit. Figures 3 and 4 show the H_{T} and $\Delta\phi_{\text{min}}(\gamma, E_{\text{T}}^{\text{miss}})$ distributions of selected diphoton events, with those of the same signal models overlaid.

To maximise the sensitivity of this analysis over a wide range of model parameters that may lead to different kinematic properties, three different signal regions (SRs) were defined based on the observed values of $E_{\text{T}}^{\text{miss}}$, H_{T} and $\Delta\phi_{\text{min}}(\gamma, E_{\text{T}}^{\text{miss}})$. SR A, optimised for gluino/squark production with a subsequent decay to a high-mass bino, requires large $E_{\text{T}}^{\text{miss}}$ and moderate H_{T}. SR B, optimised for gluino/squark production with a subsequent decay to a low-mass bino, requires moderate $E_{\text{T}}^{\text{miss}}$ and large H_{T}. SR C, optimised for the electroweak production of imtermediate-mass gaugino pairs that dominates the SPS8 cross section in this regime, requires moderate $E_{\text{T}}^{\text{miss}}$ but makes no requirement on H_{T}. In addition, a requirement of $\Delta\phi_{\text{min}}(\gamma, E_{\text{T}}^{\text{miss}}) > 0.5$ was imposed on events in SR A and C; for the low-mass bino targeted by SR B, the separation between the photon and gravitino daughters of the bino is too slight to allow for the efficient separation of signal from background through the use of this observable. The selection requirements of the three SRs are summarised in Table 1. Of the three SRs, SR A provides the greatest sensitivity to the UED model, and is thus the analysis used to test the UED model.

Table 2 shows the number of events remaining after several stages of the selection. A total of 117, 9, and 7293 candidate events were observed to pass all but the $E_{\text{T}}^{\text{miss}}$ requirement of SR A, B, and C, respectively. After imposing the final $E_{\text{T}}^{\text{miss}}$ requirement, no events remained for SR A and B, while two events remained for SR C.

Figure 5 shows the $E_{\text{T}}^{\text{miss}}$ distribution for SR C, the expected contributions from the SPS8 MC sample with $\Lambda = 190\,\text{TeV}$, and estimated background contributions from various sources (to be described below).

Table 1: Definition of the three SRs (A, B, and C) based on the quantities $\Delta\phi_{\text{min}}(\gamma, E_{\text{T}}^{\text{miss}})$, H_{T}, and $E_{\text{T}}^{\text{miss}}$.

	SR A	SR B	SR C
$\Delta\phi_{\text{min}}(\gamma, E_{\text{T}}^{\text{miss}}) >$	0.5	-	0.5
$H_{\text{T}} >$	600 GeV	1100 GeV	-
$E_{\text{T}}^{\text{miss}} >$	200 GeV	100 GeV	125 GeV

[2] An excess of events in the leading-photon spectrum for $E_{\text{T}} \sim 285\,\text{GeV}$ is observed. Searching over the range $100 < E_{\text{T}} < 500$, BumpHunter [61] finds a significance of $1.9\,\sigma$, while the local significance is found to be $\sim 3\,\sigma$. No correlation between the excess and the LHC running period or luminosity is observed. A comparison of other observables (e.g. diphoton mass, $E_{\text{T}}^{\text{miss}}$, leading-photon η, $\Delta\phi(\gamma_1, \gamma_2)$) between the excess and sideband regions exhibits no appreciable differences. We conclude that the observed excess of events is compatible with a statistical fluctuation.

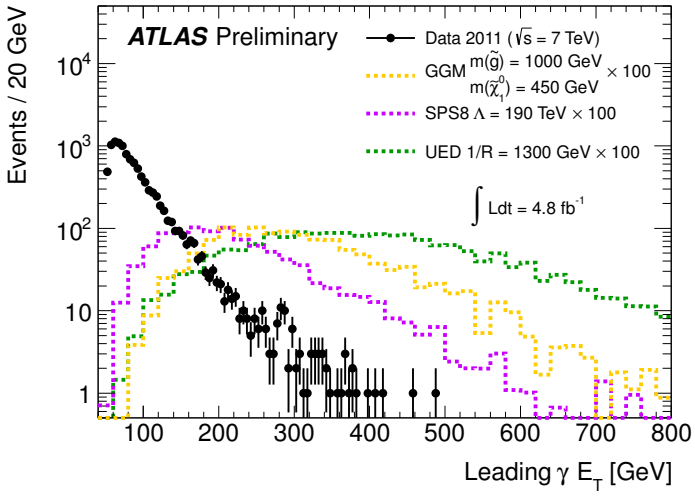

Figure 1: The E_{T} spectrum of the leading photon in the $\gamma\gamma$ candidate events in the data (points, statistical uncertainty only) together with the spectra from simulated GGM ($m_{\tilde{g}}, m_{\tilde{\chi}_1^0} = (1000, 450)\,\mathrm{GeV}$), SPS8 ($\Lambda = 190\,\mathrm{TeV}$), and UED ($1/R = 1300\,\mathrm{GeV}$) samples after the diphoton requirement. The signal samples are multiplied by a factor of 100 for visibility. See the text for more details on the excess of events for $E_{\mathrm{T}} \sim 285\,\mathrm{GeV}$.

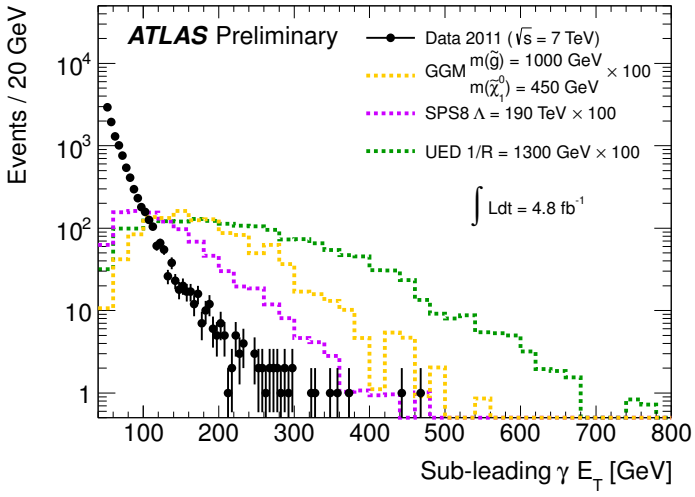

Figure 2: The E_{T} spectrum of the sub-leading photon in the $\gamma\gamma$ candidate events in the data (points, statistical uncertainty only) together with the spectra from simulated GGM ($m_{\tilde{g}}, m_{\tilde{\chi}_1^0} = (1000, 450)\,\mathrm{GeV}$), SPS8 ($\Lambda = 190\,\mathrm{TeV}$), and UED ($1/R = 1300\,\mathrm{GeV}$) samples after the diphoton requirement. The signal samples are multiplied by a factor of 100 for visibility.

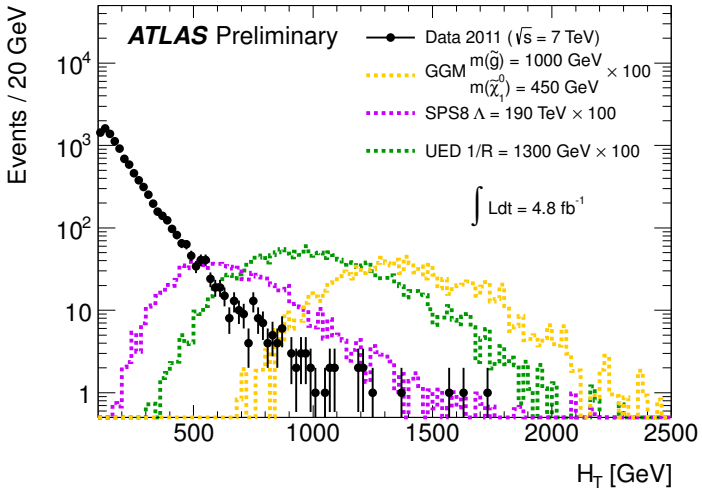

Figure 3: The H_{T} spectrum of $\gamma\gamma$ candidate events in the data (points, statistical uncertainty only) together with the spectra from simulated GGM ($m_{\tilde{g}}, m_{\tilde{\chi}_1^0} = (1000, 450)$ GeV), SPS8 ($\Lambda = 190$ TeV), and UED ($1/R = 1300$ GeV) samples after the diphoton requirement. The signal samples are multiplied by a factor of 100 for visibility.

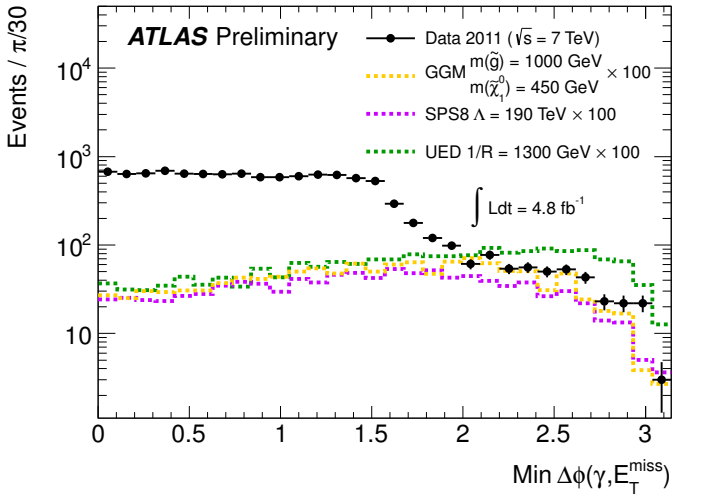

Figure 4: The minimum $\Delta\phi(\gamma, E_{\mathrm{T}}^{\mathrm{miss}})$ spectrum of $\gamma\gamma$ candidate events in the data (points, statistical uncertainty only) together with the spectra from simulated GGM ($m_{\tilde{g}}, m_{\tilde{\chi}_1^0} = (1000, 450)$ GeV), SPS8 ($\Lambda = 190$ TeV), and UED ($1/R = 1300$ GeV) samples after the diphoton requirement. The signal samples are multiplied by a factor of 100 for visibility.

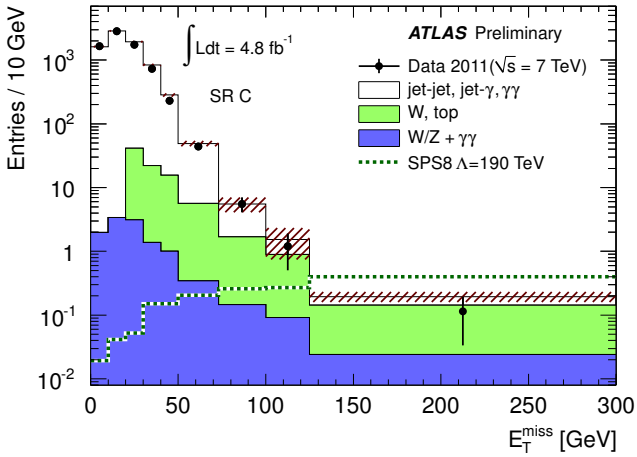

Figure 5: $E_{\mathrm{T}}^{\mathrm{miss}}$ spectra in SR C for the $\gamma\gamma$ candidate events in data (points, statistical uncertainty only) and the estimated QCD background (normalised to the number of $\gamma\gamma$ candidates with $E_{\mathrm{T}}^{\mathrm{miss}} < 20\,\mathrm{GeV}$), the $W(\rightarrow e\nu)$ + jets/γ and $t\bar{t}(\rightarrow e\nu)$ + jets backgrounds as estimated from the electron-photon control sample, and the irreducible background of $Z(\rightarrow \nu\bar{\nu})+\gamma\gamma$ and $W(\rightarrow \ell\nu)+\gamma\gamma$. The hatched region shows the uncertainty on the total background prediction. Also shown is the expected signal SPS8 ($\Lambda = 190\,\mathrm{TeV}$) sample.

8 Background estimation

Following the procedure described in Ref. [62], the contribution to the large $E_{\mathrm{T}}^{\mathrm{miss}}$ diphoton sample from SM sources can be grouped into three primary components. The first of these, referred to as "QCD background", arises from a mixture of processes that include $\gamma\gamma$ production as well as γ + jet and multijet events with at least one jet mis-reconstructed as a photon. The second background component, referred to as "EW background", is due to $W + X$ and $t\bar{t}$ events (here "X" can be any number of photons or jets), and where mis-reconstructed photons can arise from electrons and jets, and for which final-state neutrinos produce significant $E_{\mathrm{T}}^{\mathrm{miss}}$. The QCD and EW backgrounds were estimated via dedicated control samples of data events. The third background component, referred to as "irreducible", consists of W and Z bosons produced in association with two real photons, with a subsequent decay into one or more neutrinos.

To estimate the QCD background from $\gamma\gamma$, γ + jet, and multijet events, a "QCD control sample" was selected from the diphoton trigger sample by selecting events for which at least one of the photon candidates passes the loose but not the tight photon identification. Electrons were vetoed to reduce contamination from $W \rightarrow e\nu$ decays. The H_{T} and $\Delta\phi(\gamma, E_{\mathrm{T}}^{\mathrm{miss}})$ requirements associated with each of the three SRs were then applied, yielding three separate QCD control samples, or "templates". An estimate

Table 2: Samples of selected events at progressive stages of the selection. Where no number is shown the cut was not applied.

Triggered events	1166060		
Diphoton selection	10455		
	A	B	C
$\Delta\phi_{\mathrm{min}}(\gamma, E_{\mathrm{T}}^{\mathrm{miss}})$ requirement	7293	–	7293
H_{T} requirement	117	9	–
$E_{\mathrm{T}}^{\mathrm{miss}}$ requirement	0	0	2

of the QCD background contamination in each SR was obtained from imposing the $E_{\mathrm{T}}^{\mathrm{miss}}$ requirement associated with the given SR upon the corresponding QCD template, after normalising each template to the diphoton data with $E_{\mathrm{T}}^{\mathrm{miss}} < 20\,\mathrm{GeV}$ from the given SR. This yielded a QCD background expectation of $0.85 \pm 0.30(\mathrm{stat})$ events for SR C. No events above the corresponding $E_{\mathrm{T}}^{\mathrm{miss}}$ requirement are observed for the A and B control samples, yielding an estimate of 0 events with a 90 % confidence level (CL) upper limit of less than 1.01 and 1.15 background events for SR A and SR B, respectively.

To improve the constraint on the estimated background for SRs A and B, a complementary method making use of H_{T} sidebands of the QCD control sample was employed. The H_{T} requirement applied to the SR A and B QCD templates was relaxed in three steps: to 400, 200, and 0 GeV for the SR A control sample, and to 800, 400, and 200 GeV for the SR B control sample. For each SR, the $E_{\mathrm{T}}^{\mathrm{miss}}$ distribution of each of these extended control samples was scaled to the diphoton $E_{\mathrm{T}}^{\mathrm{miss}}$ distribution for $E_{\mathrm{T}}^{\mathrm{miss}} < 20\,\mathrm{GeV}$ of the given SR, yielding a series of three expected values for the QCD background as a function of the applied H_{T} requirement. The complementary estimate for the signal-region background contamination proceeded by employing a parabolic extrapolation to the actual H_{T} requirement used for the analysis (600 and 1100 GeV for SRs A and B, respectively), yielding conservative upper estimates of 0.14 and 0.54 events for SRs A and B, respectively. The overall QCD background estimates for SRs A and B were taken to be $0.07 \pm 0.07(\mathrm{syst})$ and $0.27 \pm 0.27(\mathrm{syst})$ events, respectively, half of the value of this upper estimate, with a systematic uncertainty assigned to cover the entire range between 0 and the upper estimate.

Other sources of systematic uncertainty of the estimated QCD background were considered. Using the $E_{\mathrm{T}}^{\mathrm{miss}}$ distribution from a sample of $Z \to e^+e^-$ events instead of that of the QCD sample yielded estimates of 0, 0, and 0.15 events for the SRs A, B and C, respectively. The difference between this estimate and that of the QCD sample was incorporated as a systematic error of ±0.71 on the SR C QCD background estimate. Making use of the alternative ranges $5 < E_{\mathrm{T}}^{\mathrm{miss}} < 25$ GeV and $10 < E_{\mathrm{T}}^{\mathrm{miss}} < 30$ over which the QCD sample was normalized to the $\gamma\gamma$ sample resulted in a further systematic uncertainty of ±0.03 events on the SR C QCD background estimate. The resulting QCD background estimates for the three SRs, along with their uncertainties, are compiled in Table 3.

The EW background, from $W + X$ and $t\bar{t}$ events, was estimated via an "electron-photon" control sample composed of events with at least one tight photon and one electron, each with $E_{\mathrm{T}} > 50\,\mathrm{GeV}$, and scaled by the probability for an electron to be mis-reconstructed as a tight photon, as estimated from a "tag-and-probe" study of the Z boson in the ee and $e\gamma$ sample. The scaling factor varies between 2.5 % ($0 < |\eta| < 0.6$) and 7.0 % ($1.52 < |\eta| < 1.81$), since it depends on the amount of material in front of the calorimeter. Events with two or more tight photons were vetoed from the control sample to preserve its orthogonality to the signal sample. In case of more than one electron, the one with the highest p_{T} was used.

After applying corresponding selection requirements on H_{T}, $\Delta\phi(\gamma, E_{\mathrm{T}}^{\mathrm{miss}})$, and $E_{\mathrm{T}}^{\mathrm{miss}}$, a total of 1, 3, and 26 electron-photon events were observed for the A, B, and C SRs, respectively. After multiplying by the η-dependent electron-to-photon mis-reconstruction probability, the resulting EW background contamination is estimated to be 0.03 ± 0.03, 0.09 ± 0.05 and 0.80 ± 0.16 events for SRs A, B, and C, respectively, where the uncertainties are statistical only.

The systematic error on the determination of the electron-to-photon mis-reconstruction probability is assessed by performing an independent tag-and-probe analysis with looser electron E_{T} and identification requirements. Differences with the nominal tag-and-probe analysis are taken as systematic error on the EW background estimate, resulting in relative systematic uncertainties of ±6.9%, ±7.1%, and ±10.0% for SRs A, B, and C respectively. MC studies suggest that approximately 25% of EW backgrounds involve no electron-to-photon mis-reconstruction, and thus are not accounted for with the electron-photon control sample. These events, however, typically involve a jet-to-photon mis-reconstruction, and are thus potentially accounted for in the QCD background estimate. We conservatively assign a relative

Table 3: The expected number of observed $\gamma\gamma$ events for each of the three analyses. The estimates of the irreducible background are formed from the sum of the $W(\rightarrow \ell\nu) + \gamma\gamma$ and $Z(\rightarrow \nu\bar{\nu}) + \gamma\gamma$ contributions. The uncertainties are statistical, arising from the limited statistics of the control samples, and systematic, the details of which are given in the text. For the irreducible background, the statistical uncertainty is due to limited MC statistics.

	SR A	SR B	SR C
QCD	$0.07 \pm 0.00 \pm 0.07$	$0.27 \pm 0.00 \pm 0.27$	$0.85 \pm 0.30 \pm 0.71$
Electroweak	$0.03 \pm 0.03 \pm 0.01$	$0.09 \pm 0.05 \pm 0.02$	$0.80 \pm 0.16 \pm 0.22$
$W(\rightarrow \ell\nu) + \gamma\gamma$	< 0.01	< 0.01	$0.18 \pm 0.13 \pm 0.18$
$Z(\rightarrow \nu\bar{\nu}) + \gamma\gamma$	< 0.01	< 0.01	$0.27 \pm 0.09 \pm 0.04$
Total	$0.10 \pm 0.03 \pm 0.07$	$0.36 \pm 0.05 \pm 0.27$	$2.11 \pm 0.37 \pm 0.77$
Observed events	0	0	2

systematic uncertainty of ±25% to the EW background estimates for all three SRs to account for this ambiguity. The resulting EW background estimates for the three SRs, along with their uncertainties, are compiled in Table 3.

The contribution of the irreducible background from the $Z(\rightarrow \nu\bar{\nu}) + \gamma\gamma$ and $W(\rightarrow \ell\nu) + \gamma\gamma$ processes was estimated using MC samples. It was found to be negligible for SRs A and B, and estimated to be $0.46 \pm 0.16 \pm 0.19$ events for SR C, where the first uncertainty is due to the limited statistics of the MC sample and the second to the uncertainty on the applied K-factor. These estimates, along with the resulting combined estimates for the background from all sources, are reported in Table 3.

The contamination from cosmic-ray muons, estimated using events triggered in empty LHC bunches, was found to be negligible.

9 Signal efficiencies and systematic uncertainties

The GGM signal efficiencies were determined using MC simulation over an area of the GGM parameter space that ranges from 800 GeV to 1300 GeV for the gluino (squark) mass, and from 50 GeV to within 10 GeV of the gluino (squark) mass for the neutralino mass. For SR A the efficiency increases smoothly from 1.2 % to 25 % for $(m_{\tilde{g}}, m_{\tilde{\chi}_1^0}) = (800, 50)$ GeV to $(1300, 1280)$ GeV. The efficiency drops by 5 % for the case where the gluino and neutralino masses are only separated by 10 GeV. For SR B the efficiency increases smoothly from 2.8 % to 26 % for $(m_{\tilde{g}}, m_{\tilde{\chi}_1^0}) = (800, 790)$ GeV to $(1300, 50)$ GeV. The SPS8 signal efficiency in SR C increases smoothly from 5.9 % ($\Lambda = 100$ TeV) to 21 % ($\Lambda = 250$ TeV). For SR A the UED signal efficiency, also determined using MC simulation, increases smoothly from 28 % ($1/R = 1000$ GeV) to 37 % ($1/R = 1500$ GeV).

The various relative systematic uncertainties on the GGM, SPS8, and UED signal cross sections are summarised in Table 4 for the chosen reference points: $(m_{\tilde{g}}, m_{\tilde{\chi}_1^0}) = (1000, 450)$ GeV for GGM, $\Lambda = 190$ TeV for SPS8, and $1/R = 1.3$ TeV for UED. The uncertainty on the luminosity is 3.9 % [59,60]. The trigger efficiency of the required diphoton trigger was estimated using a single photon trigger, the efficiency of which was determined using a bootstrap method [63]. The result is $99.8^{+0.2}_{-0.8}$% for events passing the diphoton selection. To estimate the systematic uncertainty due to the unknown composition of the data sample, the trigger efficiency was also evaluated on MC events using mis-reconstructed photons from filtered multijet samples and photons from signal (SUSY and UED) samples. A conservative systematic uncertainty of 0.5 % was derived from the difference between the obtained efficiencies. Uncertainties on the photon selection, the photon energy scale, and the detailed material composition of the detector, as described in Ref. [62], result in an uncertainty of 4.4 % for the GGM, SPS8 and UED

Table 4: Relative systematic uncertainties on the expected signal yield for GGM with $(m_{\tilde{g}}, m_{\tilde{\chi}_1^0}) = (1000, 450)$ GeV, SPS8 with $\Lambda = 190$ TeV, and UED with $1/R = 1.3$ TeV. For the GGM model, when the uncertainty differs for SRs A and B, it is presented as SRA/SRB. No PDF and scale uncertainties are given for the UED case as the cross section is evaluated only to LO.

Source of uncertainty	Uncertainty		
	GGM	SPS8	UED
Integrated luminosity	3.9%	3.9%	3.9%
Trigger	0.5%	0.5%	0.5%
Photon identification	4.4%	4.4%	4.4%
Photon isolation	0.9%	0.2%	0.4%
Pile-up	0.8%	0.5%	0.5%
$E_{\mathrm{T}}^{\mathrm{miss}}$ reconstruction and scale	3.9/1.1%	2.8%	1.5%
H_{T}	0.0/2.1%	–	0.4%
Signal MC statistics	3.0%	2.1%	1.4%
Total signal uncertainty	7.6/7.1%	6.8%	6.3%
PDF and scale	31%	5.5%	–
Total	32%	8.7%	6.3%

signals. The uncertainty from the photon isolation was estimated by varying the energy leakage and the pile-up corrections independently, resulting in an uncertainty of 0.9 %, 0.2 %, and 0.4 % for GGM, SPS8, and UED, respectively. The influence of pile-up on the signal efficiency, evaluated by scaling the number of pile-up events in MC by a factor of 0.9, leads to a systematic uncertainty of 0.8 % (GGM), 0.5 % (SPS8), and 0.5 % (UED). Systematic uncertainties due to the $E_{\mathrm{T}}^{\mathrm{miss}}$ reconstruction, estimated by varying the cluster energies and the $E_{\mathrm{T}}^{\mathrm{miss}}$ resolution between the measured performance and MC expectations [57], contribute an uncertainty of 0.1/0.5 % to 5.3/16.1 % (GGM, SR A/B), 1.6 % to 9.7 % (SPS8), and 0.9 % to 2 % (UED). Systematic uncertainties due to the H_{T} reconstruction, estimated by varying the energy scale and resolution of the individual objects entering H_{T}, are below 0.3 % (GGM, SR A), 0.1 % to 7.3 % (GGM, SR B), and 1.1 % to 0.1 % (UED). The systematic uncertainties from $E_{\mathrm{T}}^{\mathrm{miss}}$ and H_{T} are taken to be fully correlated. Added in quadrature, the total systematic uncertainty on the signal yield varies between 6 % and 20 % (GGM), 6 % and 15 % (SPS8), and 6 % and 7 % (UED).

The PDF and factorisation and renormalisation scale uncertainties on the GGM (SPS8) cross sections were evaluated as described in Section 4, leading to a combined systematic uncertainty between 23 – 39 %, 29–49 % and 6.3–8.3 % for the GGM (gluino), GGM (squark) and SPS8 models, respectively. The different impact of the PDF and scale uncertainties of the GGM and SPS8 yields is related to the different production mechanisms in the two models (see Section 2). In the case of UED, the PDF uncertainties were evaluated by using the `MSTW2008 LO` [64] PDF error sets in the LO cross section calculation and are about 4 %. The scale of α_s in the LO cross section calculation was increased and decreased by a factor of two, leading to a systematic uncertainty of 4.5 % and 9 %, respectively. NLO calculations are not yet available, so the LO cross sections were used for the limit calculation without any theoretical uncertainty, and the effect of PDF and scale uncertainties on the final limit is given separately.

10 Results

No evidence for physics beyond the SM was observed in any of the SRs. Based on the observed events in SR A, B and C, respectively, and the background expectation shown in Table 3, 95 % CL upper limits are set on the number of events in the different SRs from any scenario of physics beyond the SM using the

profile likelihood and CL_s prescription [65]. Uncertainties on the background and signal expectations are treated as Gaussian-distributed nuisance parameters in the maximum likelihood fit, resulting in observed upper limits of 3.1, 3.1, and 4.9 events for SRs A, B, and C, respectively. These limits translate into 95 % upper limits on the visible cross section for new physics, defined by the product of cross section, branching fraction, acceptance and efficiency for the different SR definitions, of 0.6, 0.6, and 1.0 fb, respectively. In all cases, because the observed number of signal events is close to the expected number of background events in all three SRs, expected limits on the number of events from and visible cross section for new physics are, to the quoted accuracy, identical to the observed limits.

Including the PDF and scale uncertainties on the expected cross section, which dominate the total systematic uncertainty, limits are set on the GGM squark and gluino masses. Figures 6 and 7 show the expected and observed lower limits on the GGM gluino and squark masses as a function of the neutralino mass. For comparison the lower limits from ATLAS [1] based on 1 fb^{-1} from 2011 are also shown.

Including all sources of uncertainty other than those on the PDF and renormalisation and factorisation scales, 95 % CL upper limits on the cross section of the SPS8 model are derived and displayed in Fig. 8 for the range $\Lambda = 100 - 250$ TeV along with the overall production cross section. For illustration the cross section dependence as a function of the lightest neutralino and chargino masses is also shown. Including the PDF and scale uncertainties on the cross section, a lower limit on the SPS8 breaking scale $\Lambda > 203$ TeV at 95 % CL is set.

Figure 9 shows the limit on the cross section times branching ratio for the UED model as a function of the compactification scale $1/R$. A lower 95 % CL limit of $1/R > 1.41$ TeV is set. In this case PDF and scale uncertainties are not included when calculating the limits. Including PDF and scale uncertainties computed at LO degrade the limit on $1/R$ by a few GeV.

11 Conclusions

A search for events with two photons and substantial $E_{\text{T}}^{\text{miss}}$, performed using 4.8 fb^{-1} of 7 TeV pp collision data recorded with the ATLAS detector at the LHC, is presented. The sensitivity to different new physics models producing this final state was optimised by defining three different SRs. No significant excess above the expected background is found in any SR. The results are used to set model-independent 95 % CL upper limits on possible contributions from new physics. Under the GGM hypothesis, a lower limit on the gluino/squark mass of 1.07 TeV/0.91 TeV is determined for bino masses above 50 GeV. A lower limit of 203 TeV is set on the SPS8 breaking scale Λ, and a lower limit of 1.41 TeV is set on the UED compactification scale $1/R$.

References

[1] ATLAS Collaboration, *Search for Diphoton Events with Large Missing Transverse Momentum in 1 fb^{-1} of 7 TeV Proton-Proton Collision Data with the ATLAS Detector*, Phys. Lett. **B710** (2012) 519, arXiv:1111.4116 [hep-ex].

[2] P. Meade, N. Seiberg, and D. Shih, *General Gauge Mediation*, Prog. Theor. Phys. Suppl. **177** (2009) 143, arXiv:0801.3278 [hep-ph].

[3] M. Buican, P. Meade, N. Seiberg, and D. Shih, *Exploring General Gauge Mediation*, JHEP **03** (2009) 016, arXiv:0812.3668 [hep-ph].

[4] J. T. Ruderman and D. Shih, *General Neutralino NLSPs at the Early LHC*, arXiv:1103.6083 [hep-ph].

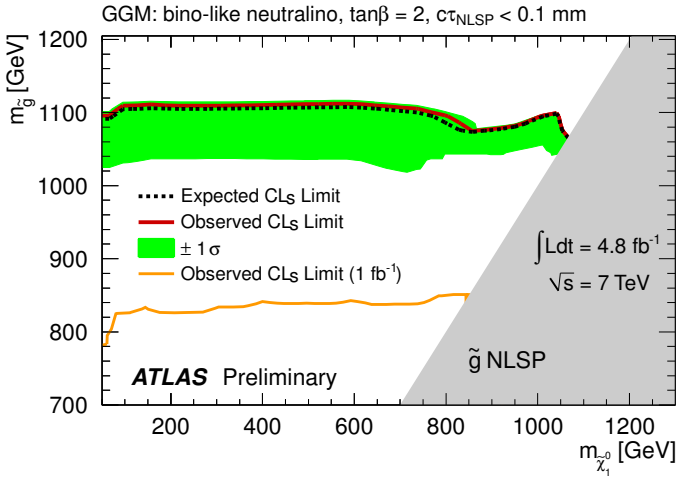

Figure 6: Expected and observed 95 % CL lower limits on the gluino mass as a function of the neutralino mass in the GGM model with a bino-like lightest neutralino NLSP (the grey area indicates the region where the NLSP is the gluino, which is not considered here). The other sparticle masses are decoupled. Further model parameters are $\tan\beta = 2$ and $c\tau_{\mathrm{NLSP}} < 0.1$ mm. The previous ATLAS [1] limit is also shown.

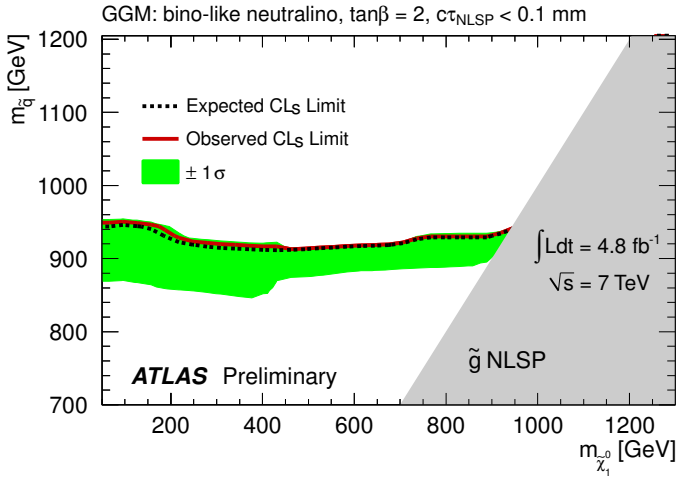

Figure 7: Expected and observed 95 % CL lower limits on the squark mass as a function of the neutralino mass in the GGM model with a bino-like lightest neutralino NLSP (the grey area indicates the region where the NLSP is the gluino, which is not considered here). The other sparticle masses are decouled. Further model parameters are $\tan\beta = 2$ and $c\tau_{\mathrm{NLSP}} < 0.1$ mm.

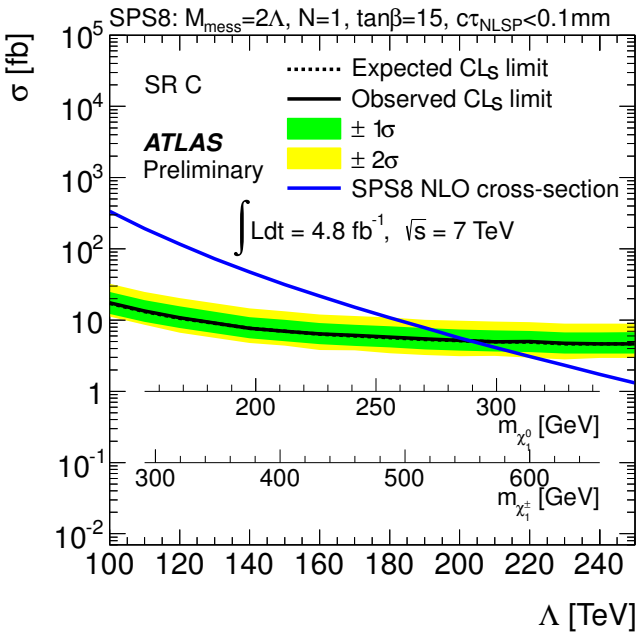

Figure 8: Expected and observed 95 % CL upper limits on the sparticle production cross section in the SPS8 model, and the NLO cross section prediction, as a function of Λ and the lightest neutralino and chargino masses. Further SPS8 model parameters are $M_{\text{mess}} = 2\Lambda$, $N_5 = 1$, $\tan\beta = 15$, and $c\tau_{\text{NLSP}} < 0.1$ mm. Limits are set based on SR C.

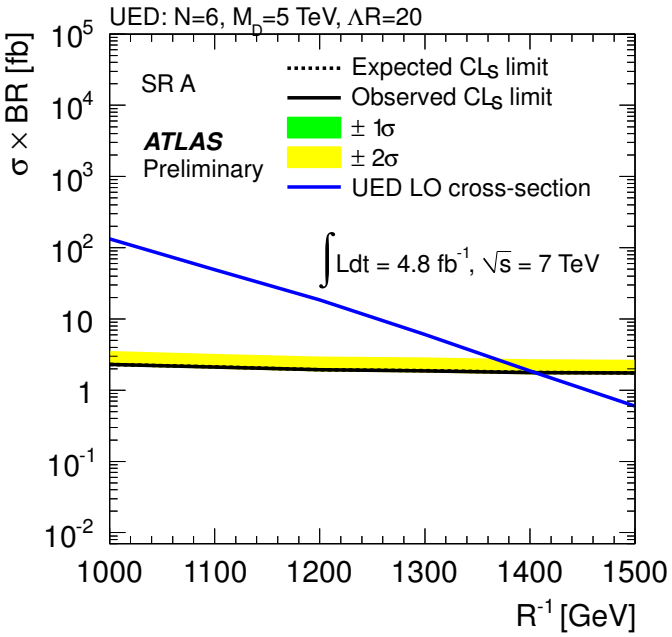

Figure 9: Expected and observed 95 % CL upper limits on the KK particle production cross section times branching fraction to two photons in the UED model, and the LO cross section prediction times branching fraction, as a function of $1/R$. The UED model parameters are $N = 6$, $M_D = 5$ TeV, and $\Lambda R = 20$. Limits are set based on SR A.

[5] B. C. Allanach et al., *The Snowmass Points and Slopes: Benchmarks for SUSY Searches*, Eur. Phys. J. **C25** (2002) 113, arXiv:hep-ph/0202233.

[6] T. Appelquist, H.-C. Cheng, and B. A. Dobrescu, *Bounds on Universal Extra Dimensions*, Phys. Rev. **D64** (2001) 035002, arXiv:hep-ph/0012100.

[7] C. Macesanu, C. McMullen, and S. Nandi, *New Signal for Universal Extra Dimensions*, Phys. Lett. **B546** (2002) 253, arXiv:hep-ph/0207269.

[8] C. Macesanu, *The Phenomenology of Universal Extra Dimensions at Hadron Colliders*, Int. J. Mod. Phys. **A21** (2006) 2259, arXiv:hep-ph/0510418.

[9] H. Miyazawa, *Baryon Number Changing Currents*, Prog. Theor. Phys. **36 (6)** (1966) 1266.

[10] P. Ramond, *Dual Theory for Free Fermions*, Phys. Rev. **D3** (1971) 2415.

[11] Y. A. Gol'fand and E. P. Likhtman, *Extension of the Algebra of Poincare Group Generators and Violation of p Invariance*, JETP Lett. **13** (1971) 323. [Pisma Zh.Eksp.Teor.Fiz.13:452-455,1971].

[12] A. Neveu and J. H. Schwarz, *Factorizable Dual Model of Pions*, Nucl. Phys. **B31** (1971) 86.

[13] A. Neveu and J. H. Schwarz, *Quark Model of Dual Pions*, Phys. Rev. **D4** (1971) 1109.

[14] J. Gervais and B. Sakita, *Field Theory Interpretation of Supergauges in Dual Models*, Nucl. Phys. **B34** (1971) 632.

[15] D. V. Volkov and V. P. Akulov, *Is the Neutrino a Goldstone Particle?*, Phys. Lett. **B46** (1973) 109.

[16] J. Wess and B. Zumino, *A Lagrangian Model Invariant Under Supergauge Transformations*, Phys. Lett. **B49** (1974) 52.

[17] J. Wess and B. Zumino, *Supergauge Transformations in Four-Dimensions*, Nucl. Phys. **B70** (1974) 39.

[18] P. Fayet, *Supersymmetry and Weak, Electromagnetic and Strong Interactions*, Phys. Lett. **B64** (1976) 159.

[19] P. Fayet, *Spontaneously Broken Supersymmetric Theories of Weak, Electromagnetic and Strong Interactions*, Phys. Lett. **B69** (1977) 489.

[20] G. R. Farrar and P. Fayet, *Phenomenology of the Production, Decay, and Detection of New Hadronic States Associated with Supersymmetry*, Phys. Lett. **B76** (1978) 575.

[21] P. Fayet, *Relations Between the Masses of the Superpartners of Leptons and Quarks, the Goldstino Couplings and the Neutral Currents*, Phys. Lett. **B84** (1979) 416.

[22] S. Dimopoulos and H. Georgi, *Softly Broken Supersymmetry and SU(5)*, Nucl. Phys. **B193** (1981) 150.

[23] M. Dine and W. Fischler, *A Phenomenological Model of Particle Physics Based on Supersymmetry*, Phys. Lett. **B110** (1982) 227.

[24] L. Alvarez-Gaume, M. Claudson, and M. B. Wise, *Low-Energy Supersymmetry*, Nucl. Phys. **B207** (1982) 96.

[25] C. R. Nappi and B. A. Ovrut, *Supersymmetric Extension of the SU(3) x SU(2) x U(1) Model*, Phys. Lett. **B113** (1982) 175.

[26] M. Dine and A. E. Nelson, *Dynamical Supersymmetry Breaking at Low-energies*, Phys. Rev. **D48** (1993) 1277, arXiv:hep-ph/9303230.

[27] M. Dine, A. E. Nelson, and Y. Shirman, *Low-Energy Dynamical Supersymmetry Breaking Simplified*, Phys. Rev. **D51** (1995) 1362, arXiv:hep-ph/9408384.

[28] M. Dine, A. E. Nelson, Y. Nir, and Y. Shirman, *New Tools for Low-Energy Dynamical Supersymmetry Breaking*, Phys. Rev. **D53** (1996) 2658, arXiv:hep-ph/9507378.

[29] ATLAS Collaboration, *Search for Events with Large Missing Transverse Momentum, Jets, and at Least Two Tau Leptons in 7 TeV Proton-Proton Collision Data with the ATLAS Detector*, arXiv:1203.6580 [hep-ex]. Submitted to PLB.

[30] ATLAS Collaboration, *Search for Supersymmetry with Jets, Missing Transverse Momentum and at Least One Hadronically Decaying Tau Lepton in Proton-Proton Collisions at* $\sqrt{s} = 7$ *TeV with the ATLAS Detector*, arXiv:1204.3852 [hep-ex]. Submitted to PLB.

[31] CMS Collaboration, *Search for Supersymmetry in Events with a Lepton, a Photon, and Large Missing Transverse Energy in pp Collisions at* $\sqrt{s} = 7$ *TeV*, JHEP **1106** (2011) 093, arXiv:1105.3152 [hep-ex].

[32] C. Macesanu, C. McMullen, and S. Nandi, *Collider Implications of Universal Extra Dimensions*, Phys. Rev. **D66** (2002) 015009, arXiv:hep-ph/0201300.

[33] A. De Rujula, A. Donini, M. Gavela, and S. Rigolin, *Fat Brane Phenomena*, Phys. Lett. **B482** (2000) 195, arXiv:hep-ph/0001335.

[34] H.-C. Cheng, K. T. Matchev, and M. Schmaltz, *Radiative Corrections to Kaluza-Klein Masses*, Phys. Rev. **D66** (2002) 036005, arXiv:hep-ph/0204342 [hep-ph].

[35] M. ElKacimi, D. Goujdami, H. Przysiezniak, and P. Z. Skands, *One Universal Extra Dimension in Pythia*, Comput. Phys. Commun. **181** (2010) 122, arXiv:0901.4087 [hep-ph].

[36] A. Djouadi, J.-L. Kneur, and G. Moultaka, *SuSpect: A Fortran Code for the Supersymmetric and Higgs Particle Spectrum in the MSSM*, Comput. Phys. Commun. **176** (2007) 426, arXiv:hep-ph/0211331.

[37] M. Muhlleitner, A. Djouadi, and Y. Mambrini, *SDECAY: A Fortran Code for the Decays of the Supersymmetric Particles in the MSSM*, Comput. Phys. Commun. **168** (2005) 46, arXiv:hep-ph/0311167.

[38] F. E. Paige, S. D. Protopopescu, H. Baer, and X. Tata, *ISAJET 7.69: A Monte Carlo Event Generator for pp,* $\bar{p}p$*, and* e^+e^- *Reactions*, arXiv:hep-ph/0312045.

[39] M. Bahr et al., *Herwig++ Physics and Manual*, Eur. Phys. J. **C58** (2008) 639, arXiv:0803.0883 [hep-ph].

[40] A. Sherstnev and R. S. Thorne, *Parton Distributions for LO Generators*, Eur. Phys. J. **C55** (2008) 553, arXiv:0711.2473 [hep-ph].

[41] W. Beenakker, R. Hopker, M. Spira, and P. Zerwas, *Squark and Gluino Production at Hadron Colliders*, Nucl. Phys. **B492** (1997) 51, arXiv:hep-ph/9610490.

[42] A. Kulesza and L. Motyka, *Threshold Resummation for Squark-Antisquark and Gluino-pair Production at the LHC*, Phys. Rev. Lett. **102** (2009) 111802, arXiv:0807.2405 [hep-ph].

[43] A. Kulesza and L. Motyka, *Soft Gluon Resummation for the Production of Gluino-Gluino and Squark-Antisquark Pairs at the LHC*, Phys. Rev. **D80** (2009) 095004, arXiv:0905.4749 [hep-ph].

[44] W. Beenakker et al., *Soft-Gluon Resummation for Squark and Gluino Hadroproduction*, JHEP **0912** (2009) 041, arXiv:0909.4418 [hep-ph].

[45] W. Beenakker et al., *Squark and Gluino Hadroproduction*, Int. J. Mod. Phys. **A26** (2011) 2637–2664, arXiv:1105.1110 [hep-ph].

[46] M. Kramer et al., *Supersymmetry Production Cross Sections in pp Collisions at* $\sqrt{s} = 7$ *TeV*, arXiv:1206.2892 [hep-ph].

[47] T. Sjostrand, S. Mrenna, and P. Skands, *PYTHIA 6.4 Physics and Manual*, JHEP **05** (2006) 026, arXiv:hep-ph/0603175.

[48] J. Alwall et al., *MadGraph/MadEvent v4: The New Web Generation*, JHEP **09** (2007) 028, arXiv:0706.2334 [hep-ph].

[49] D. Stump et al., *Inclusive Jet Production, Parton Distributions, and the Search for New Physics*, JHEP **10** (2003) 046, arXiv:hep-ph/0303013.

[50] G. Bozzi, F. Campanario, M. Rauch, and D. Zeppenfeld, *$Z\gamma\gamma$ Production with Leptonic Decays and Triple Photon Production at NLO QCD*, Phys.Rev. **D84** (2011) 074028, arXiv:1107.3149 [hep-ph].

[51] G. Bozzi, F. Campanario, M. Rauch, and D. Zeppenfeld, *$W\gamma\gamma$ Production with Leptonic Decays at NLO QCD*, Phys. Rev. **D83** (2011) 114035, arXiv:1103.4613 [hep-ph].

[52] GEANT4 Collaboration, S. Agostinelli et al., *GEANT4: A Simulation Toolkit*, Nucl. Instrum. Meth. **A506** (2003) 250.

[53] ATLAS Collaboration, *The ATLAS Simulation Infrastructure*, Eur. Phys. J. **C70** (2010) 823, arXiv:1005.4568 [physics.ins-det].

[54] ATLAS Collaboration, *The ATLAS Experiment at the CERN Large Hadron Collider*, JINST **3** (2008) S08003.

[55] ATLAS Collaboration, *Measurement of the Inclusive Isolated Prompt Photon Cross Section in pp Collisions at* $\sqrt{s} = 7$ *TeV with the ATLAS Detector*, Phys. Rev. **D83** (2011) 052005, arXiv:1012.4389 [hep-ex].

[56] ATLAS Collaboration, *Electron Performance Measurements with the ATLAS Detector Using the 2010 LHC Proton-Proton Collision Data*, Eur. Phys. J. **C72** (2012) 1909, arXiv:1110.3174 [hep-ex].

[57] ATLAS Collaboration, *Performance of Missing Transverse Momentum Reconstruction in Proton-Proton Collisions at 7 TeV with ATLAS*, Eur. Phys. J. **C72** (2012) 1844, arXiv:1108.5602 [hep-ex].

[58] M. Cacciari, G. Salam, and G. Soyez, *The Anti-k_t Jet Clustering Algorithm*, JHEP **04** (2008) 063, arXiv:0802.1189.

[59] ATLAS Collaboration, *Luminosity Determination in pp Collisions at $\sqrt{s} = 7$ TeV Using the ATLAS Detector at the LHC*, Eur. Phys. J. **C71** (2011) 1630, arXiv:1101.2185 [hep-ex].

[60] ATLAS Collaboration, *Luminosity Determination in pp Collisions at $\sqrt{s} = 7$ TeV Using the ATLAS Detector in 2011*, ATLAS-CONF-2011-116. http://cdsweb.cern.ch/record/1376384.

[61] G. Choudalakis, *On Hypothesis Testing, Trials Factor, Hypertests and the BumpHunter*, arXiv:1101.0390 [physics.data-an].

[62] ATLAS Collaboration, *Search for Diphoton Events with Large Missing Transverse Energy with 36 pb^{-1} of 7 TeV Proton-Proton Collision Data with the ATLAS Detector*, Eur. Phys. J. **C71** (2011) 1744, arXiv:1107.0561 [hep-ex].

[63] ATLAS Collaboration, *Performance of the ATLAS Trigger System in 2010*, Eur. Phys. J. **C72** (2012) 1849, arXiv:1110.1530 [hep-ex].

[64] A. Martin, W. Stirling, R. Thorne, and G. Watt, *Parton Distributions for the LHC*, Eur. Phys. J. **C63** (2008) 189, arXiv:0901.0002 [hep-ph].

[65] A. L. Read, *Presentation of Search Results: The CL_s Technique*, J. Phys. **G28** (2002) 2693.